Dentomaxillofacial Radiology (2014) 43, 20140019

birpublications.org/dmfr

TECHNICAL REPORT

Assessment of metal artefact reduction around dental titanium implants in cone beam CT

[1]A Parsa, [1]N Ibrahim, [2]B Hassan, [1]K Syriopoulos and [1]P van der Stelt

[1]*Department of General and Specialized Dentistry, Section Oral and Maxillofacial Radiology, Academic Center for Dentistry Amsterdam (ACTA), Amsterdam, Netherlands;* [2]*Department of Oral Implantology and Prosthetic Dentistry, Academic Center for Dentistry Amsterdam (ACTA), Amsterdam, Netherlands*

Objectives: The aim of this study was to investigate if the metal artefact reduction (MAR) tool used in the software of the ORTHOPANTOMOGRAPH® OP300 (Instrumentarium Dental, Tuusula, Finland) can improve the gray value levels in post-operative implant scans.
Methods: 20 potential implant sites were selected from 5 edentulous human dry mandibles. Each mandible was scanned by a CBCT scanner, and images were produced under three different conditions: implant sites drilled but no implants inserted, implants inserted without application of MAR and implants inserted with application of MAR. Using Geomagic® Studio 2012 (Geomagic, Morrisville, NC) and 3Diagnosys® v. 5.3.1 (3Diemme® SRL, Cantù, Italy) software, three scans of each mandible were superimposed. The mean gray value of identical regions of bone around the implants was derived for each condition. The differences between gray value measurements at implant sites derived from different conditions were assessed.
Results: A significant difference was found between mean gray values from the scans with no implants inserted and with implants inserted (with and without MAR) ($p = 0.012$). No significant difference was revealed for gray values measured from scans with and without MAR ($p = 0.975$).
Conclusions: The MAR tool in the software of the ORTHOPANTOMOGRAPH OP300 CBCT scanner does not significantly correct the voxel gray values affected by the metal artefact in the vicinity of an implant in human dry mandibles.
Dentomaxillofacial Radiology (2014) **43**, 20140019. doi: 10.1259/dmfr.20140019

Cite this article as: Parsa A, Ibrahim N, Hassan B, Syriopoulos K, van der Stelt P. Assessment of metal artefact reduction around dental titanium implants in cone beam CT. *Dentomaxillofac Radiol* 2014; **43**: 20140019.

Keywords: cone beam computed tomography; artefacts; dental implants; titanium

Introduction

CBCT has become the imaging modality of choice in dental implantology. Because of its high accuracy for linear measurements, bone height, width and the proximity to adjacent normal anatomic structures, such as the maxillary sinus or the inferior dental canal, can be precisely evaluated.[1] Additionally, bone quality evaluated by CBCT has been shown to have a good correlation with the primary implant stability.[2]

Correspondence to: Dr Azin Parsa. E-mail: a.parsa@acta.nl
Received 17 January 2014; revised 6 August 2014; accepted 13 August 2014

Although CBCT has several advantages over multislice CT (MSCT), metal artefacts caused by titanium implants in the path of the radiation can significantly deteriorate the diagnostic image quality.[3,4] An implant can induce dark artefacts, induced by scattering, and streak artefacts,[4] making anatomical structures ambiguous and influencing the contrast between adjacent regions. These effects can seriously interfere with the diagnostic yield of an image.[5]

Most of the studies on metal artefact reduction (MAR) have focused on MSCT scanners. Two methods for MAR

in MSCT have been described: projection adjustment[6–8] and reconstruction enhancement.[9,10] As both MSCT and CBCT scanners use the backprojection algorithm for image acquisition,[11] CT MAR methods could be modified for use in CBCT. One of the methods is based on pre-reconstruction of the volume followed by segmenting the metal objects[3] and removing metal regions in the two-dimensional projections concerned.[12]

Recently, some manufacturers made MAR options available in CBCT machines.[13–15] Previous *ex vivo* studies on the efficacy of MAR visually assessed the area adjacent to dense foreign objects.[13,14] The ORTHOPANTOMOGRAPH® OP300 (Instrumentarium Dental, Tuusula, Finland), which combines a panoramic imaging system with cone beam and three dimension, is a newly developed platform with the MAR tool. The aim of this study was to investigate if the MAR tool in CBCT would remove the metal artefacts around dental titanium implants.

Methods and materials

Sample preparation and radiographic evaluation

Five edentulous human dry mandibles (without soft tissue or any soft-tissue equivalent materials) not identified by age, sex or ethnic group were obtained from the Department of Functional Anatomy, at the Academic Centre for Dentistry. The use of this human material was approved by the local ethical committee. In total, 20 potential implant sites were selected in the lateral incisor and first pre-molar regions. An osteotomy was prepared using a twisted drill (Straumann®, Basel, Switzerland) for each available implant of size 4.1 mm. In total, four holes were prepared in each mandible. Prior to implant insertion, the drilled mandibles were scanned by the ORTHOPANTOMOGRAPH OP300 CBCT [90 kVp; 10 mA; exposure time, 2.3 s; field of view (FOV), 6×4 cm; and depth, 14 bit]. Following the insertion of each individual implant, two more CBCT scans were made: with standard settings and applying the MAR tool. The position of each mandible within the selected FOV was identical in the three scans of each implant site. In all CBCT scans, the lower border of the mandible was parallel to the floor. In this study, we named the scans without implant as Condition 1, scans with implant inserted and deactivated MAR as Condition 2 and scans with implant and MAR option as Condition 3.

Image processing

CBCT data sets were converted to digital imaging and communications in medicine format 3 data sets. Further analysis of data was executed with Geomagic® Studio 2012 (Geomagic, Morrisville, NC) and 3Diagnosys® v. 5.3.1 (3Diemme® SRL, Cantù, Italy). Condition 2 scans were imported to 3Diagnosys. These scans were considered as reference scans for each implant site in order to select an identical region from all conditions (and not as reference for data analysis). A region with truncated conical shape (diameter of 4–5 mm and height of 5 mm) surrounding the implant was selected manually as a virtual probe (Figure 1). The axis of the selected region and the axis of the implant were identical. This truncated cone was totally within the bone and was used to select a region of interest (ROI) in the immediate vicinity of each implant. The reason for selecting Condition 2 as the reference scan was that we aimed to have the ROIs around the implants as identical as possible. Owing to the differences between the length of drilled holes and implants, it was not possible to achieve this aim in Condition 1. Although, metal artefacts in Condition 2, made the selection of ROI difficult. However, considering the implant body as a reference for selection of ROI allowed us to ignore the shape, size and position of drilled sites in Condition 1. Therefore, we found the implant body as the better option to select the ROI around it rather than the drilled site. It must be emphasized that owing to severe metal artefacts around some implants in Condition 2, there was a possibility to have a distance (maximum, 0.5 mm) between the probe and the implant, which could affect the accuracy of our results. The mean gray value of a ROI with 1-mm thickness around the probe was derived (Figure 2). The selected ROI had a volume of 86.4 mm^3 including 10,800 voxels. The surface of the mandible and of the inserted probe was generated and exported as standard triangulation language (STL) files. The other two scans of the same implant site (Conditions 1 and 3) were imported into 3Diagnosys and also converted into STL files. To transfer the probe from scan Condition 2 to the same site in the scans of the other two conditions, an observer-independent and automated three-dimensional (3D) superimposition algorithm was applied to the STL files of the probe and reference scan and to the scans of Conditions 1 and 3 successively using the Geomagic software. To apply this 3D matching, a "best-fit alignment" tool was used. This procedure consisted of the movement of the surface of a reference scan (Condition 2) to share its physical space with the STL of the mandible of Conditions 1 and 3. In Geomagic, the best-fit alignment operates in two automated phases. In the first phase or "initial gross alignment phase", two objects are matched roughly using a few points of comparison. In the second phase, which is the "fine adjustment phase", a higher number of points of comparison are used for an optimized superimposition. Following these alignment approaches, the scans of the different conditions were matched. In the matching procedures, the reference STL was set as a floating model and the other one as fixed. The transformation matrix of the reference STL representing its cumulative change in position relative to the original position was saved. Then, this transformation matrix was loaded and applied to the probe to transfer it from the reference image to the same region of the other STL. This 3D registration was used to standardize the selection of ROIs to ensure that the voxel gray value measurements are exactly from the same site. The transformed probe was saved as a new STL and exported

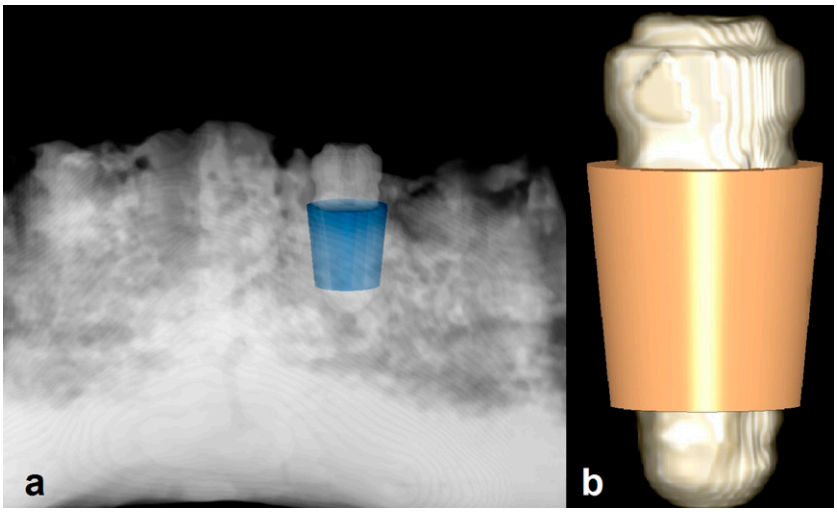

Figure 1 (a) An example of selecting a region with truncated conical shape (radius of 4 and 5 mm and height of 5 mm) surrounding an implant, and (b) a three-dimensional reconstruction of an implant with a region of interest.

to 3Diagnosys with the corresponding scan. The scan including the transformed probe was analysed, and an area with 1-mm thickness was selected around the virtual probe. The mean voxel gray value of the selected ROI around the probe was exported.

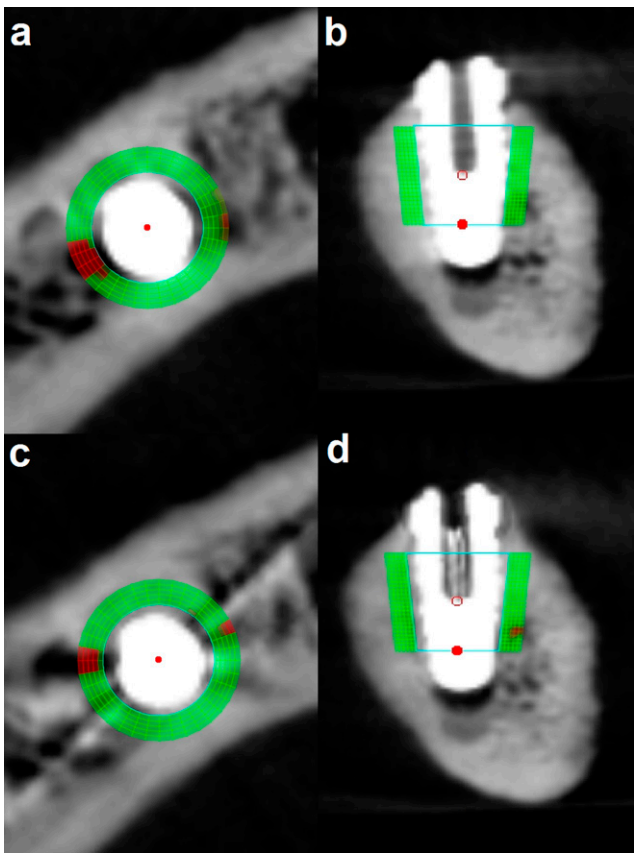

Figure 2 Measurement of an area with 1-mm thickness around the probe. (a, b) axial and sagittal views without metal artefact reduction (MAR) mode and (c, d) axial and sagittal views with MAR mode.

The method as described was applied at each implant site to derive the mean gray values of identical regions for the three different scan conditions. Applied image processing in this study included two phases: manual and automated. The insertion of the probe around each implant in Condition 2 was performed by the observer (manually) and in the second phase, which consisted of the registration of Conditions 1 and 3 scans on Condition 2 scan as well as the gray value measurements, was performed by the software (observer independent).

The gray value measurements of the ROIs in Condition 2 and registration and the gray value measurements of Conditions 1 and 3 were performed three times with 2-week intervals to assess the reproducibility. Thus, in total, at each implant site, nine mean gray values were derived.

Data analysis

The study design included scan conditions (3 selections) and implant sites (20 selections) as fixed variables, and the measurement for Conditions 1, 2 and 3 (3 times) as the repeated factor (Table 1). The UNIANOVA procedure of SPSS® v. 20.0 (SPSS Inc., Chicago, IL) was used for the statistical analysis. First, the reproducibility of the gray value measurements was assessed. Thereafter, the possible differences between the gray values derived from Condition 1 and the mean of Conditions 2 and 3, and then between gray values of Conditions 2 and 3 were evaluated.

Results

Repeated measurements for Condition 2 showed exactly identical numbers. Statistical analysis of repeated measured gray values revealed no statistical significant difference for both Condition 1 and 3 scans (Cronbach's

Table 1 Gray value measurements derived from Conditions 1–3

	Condition 1, gray value			*Condition 2, gray value*	*Condition 3, gray value*		
Implant site number	*First measurement*	*Second measurement*	*Third measurement*	*First, second and third measurements*	*First measurement*	*Second measurement*	*Third measurement*
1	576.74	658.68	581.06	866.01	838.30	843.33	829.18
2	883.03	913.32	893.20	1002.62	1023.41	1035.60	994.09
3	713.50	736.79	720.87	883.81	975.59	953.08	940.30
4	428.17	453.52	459.92	588.81	555.84	549.52	556.37
5	758.19	766.84	765.73	974.77	927.45	934.62	915.37
6	720.01	716.17	758.41	844.28	834.96	830.15	817.53
7	583.47	618.31	606.84	828.25	804.71	789.37	817.01
8	41.49	52.02	63.83	177.82	227.09	232.28	211.81
9	471.48	478.67	496.58	619.36	553.19	564.26	574.85
10	822.17	805.53	829.66	1004.07	985.60	986.32	990.23
11	256.33	275.00	277.70	489.95	488.68	451.42	468.69
12	594.57	603.55	588.27	791.65	806.46	805.80	807.18
13	548.38	548.91	556.50	712.65	685.96	698.87	718.20
14	579.31	588.54	583.60	706.45	719.70	710.70	721.71
15	744.50	733.21	721.82	832.06	821.19	803.04	820.10
16	428.77	450.47	442.87	710.56	694.23	710.69	708.08
17	38.48	55.97	29.82	248.09	207.25	217.66	224.43
18	432.27	421.75	418.33	593.09	656.80	688.49	663.37
19	704.34	695.25	687.63	765.19	767.95	781.58	750.58
20	376.38	386.82	363.72	469.43	506.42	495.81	500.10

alpha = 0.99). Assessing the reproducibility of Conditions 1 and 3 showed the Cronbach's alpha as almost perfect, which means that there is almost no error in the repeated measurements. Table 2 shows the mean and standard of deviation of gray value measurements for each repetition of Conditions 1–3. The mean of repeated measurements of each implant site was calculated for further analysis. The mean gray values ranged from 41.42 to 896.52 (mean, 541.79 and standard deviation, 231.92), from 177.82 to 1004.07 (mean, 705.45 and standard deviation, 228.54) and from 216.44 to 1017.70 (mean, 703.21 and standard deviation, 225.86), respectively, for Conditions 1–3. Condition 1 mean gray values were considerably lower than those of Conditions 2 and 3. The UNIANOVA test showed a significant difference between Condition 1 and the mean of Conditions 2 and 3 ($p = 0.012$). No significant difference between gray values measured from Conditions 2 and 3 ($p = 0.975$) was revealed.

Discussion

Although pre-operative planning of implant placement remains the main diagnostic indication for CBCT, in recent years there has been an increasing interest in applying CBCT to assess and follow-up peri-implant osseous hard tissue changes especially in the aesthetic zone where resorption of the thin facial buccal bone plate is a main concern. Additionally, several reports have proven the potential of applying CBCT for assessing bone to implant contact.[16,17]

However, the main limitation of any 3D radiographic modality, which operates with polychromatic X-ray beam and uses backprojection algorithm for 3D reconstruction in assessing areas around an implant, is that the closer an observer gets to the implant surface the less reliable the reconstruction is.[11] In current CBCT scanners, beam hardening from an existing implant severely affects the reconstruction reliability and complicates the visualization of bone to implant contact. This observed difference can be explained based on the mathematical theory of variability in the coefficient of X-ray absorption between implant and bone. Thus, a reliable artefact reduction must be based on more sophisticated algorithm for pre-processing of the actual physical image acquisition rather than on post processing of affected data by beam hardening.[11] Several techniques have been applied for MAR in image reconstruction, which can be mainly divided into pre- and post-processing algorithms. In pre-processing algorithm, the metal part in the basis projections data set is located, and then using the interpolation algorithm, the metal projection data are processed. Finally from the pre-processed data sets, CT axial images are reconstructed, and the metal section is retrieved.[12] Post-processing algorithm is based on segmentation and modification of metal areas in each projection image, and reconstruction of the final CT image with the modified data. However, owing to the proximity of bone and metal gray values in certain regions, it is hard to build an algorithm for an accurate metal segmentation.[12] Image

Table 2 Mean and standard deviation (SD) of gray values for the repeated measurements of Conditions 1–3 at each implant site

Condition	*Repetition*	*Mean*	*SD*
1	First	535.08	233.06
1	Second	547.97	231.39
1	Third	542.32	232.25
2	First, second and third	705.45	228.54
3	First	704.04	227.79
3	Second	704.13	227.53
3	Third	701.46	222.89

quality was found to be higher upon employing pre- rather than post-processing algorithms.[18] Although the Instrumentarium company (Tuusula, Finland) was requested to provide us with brief information with regard to applied MAR algorithm, the inner workings of the algorithm as well as whether the algorithm is a pre- or a post-processing one were unfortunately unavailable owing to patenting and copyright issues.

Therefore, it is scientifically relevant to assess whether CBCT can indeed be applied to these indications and crucially whether image quality can be improved through the use of MAR tools to be able to visualize bone in the presence of an existing implant. Of course, titanium implants remain the most popular despite the recent introduction of zirconium or ceramic implants and therefore titanium implants were selected to mimic the real clinical situation. Metallic objects such as titanium dental implants in the FOV can cause artefacts consisting three elementary sources: photon starvation, scattering and beam hardening.[19] The density of these materials is not in the normal range that is suitable for CBCT scans. Therefore, an implant can completely absorb the X-ray beam, leading to incorrectly higher gray values around the implant site.[20] These hyperdense lines that spread out horizontally from the implants are called streak artefacts. However, an implant can also harden the energy of the X-ray beam passing through and cause dark zones adjacent to the implant, mimicking a bone defect or loss of osseointegration.[14] Although some manufacturers provide metal artefact reduction software to improve the image quality at implant sites, its clinical application is limited owing to the loss of details in the neighbourhood of the implants.[20] As an earlier attempt to assess the effect of MAR, two *in vitro* studies using the Picasso Master 3D® (Vatech, Hwaseong, Republic of Korea) revealed improvements of image quality when the MAR tool was used in the presence of metallic objects. The MAR software was able to increase the contrast-to-noise ratio and decrease the gray value variation.[15,18] Gutta-percha, which is used for endodontic treatment, has also a high density that can induce artefacts.[21] The artefacts may degrade the diagnostic accuracy and impair the detection of a root fracture. The efficiency of MAR in root fracture detection (in endodontically treated teeth) was evaluated in a recent study. The results for the two CBCT scanners included in this study, ProMax® (Planmeca, Helsinki, Finland) and Picasso Master 3D, showed higher accuracy in scans without the MAR option.[13] However, another study on the Planmeca ProMax showed no difference in the detection of peri-implant and buccal periodontal defects among CBCT images with and without the MAR mode activated.[14]

Although different CBCT scanners show a wide range of gray value variations of voxels at regions in the vicinity of an implant site, increasing the milliampere second and the size of the FOV may decrease this variation in some scanners.[22] However, it can boost the X-ray dose absorbed by the patient. In theory, increasing the tube potential can improve the attenuation by materials with high density,[11] but practically it cannot decrease metal artefacts.[23] Therefore, it seems that pre- and post-processing algorithms can be better approaches for metal artefact reduction in dental CBCT devices.[9,15] It should be emphasized that "sophisticated mathematical modeling" of image acquisition is superior to post-processing algorithms. No matter which post-processing algorithm is applied, there is always missed data that cannot be corrected but only estimated.[11]

To the best of our knowledge there has been no report on the application of the MAR tool in the ORTHOPANTOMOGRAPH OP300. However, as the algorithm applied for metal artefact reduction in the mentioned scanner is not known, there is a possibility that a similar MAR tool is present in other brands of CT or CBCT. The current *ex vivo* study showed that gray voxel values around an implant significantly deviate from the original range regardless of the application of the MAR tool. The results showed no difference in gray value ranges at peri-implant sites with and without the application of MAR mode in the CBCT scanner mentioned in this study. It should be emphasized that this study focused on the gray value changes in the vicinity of an existing implant. The gray values were assessed to evaluate the level of image degradation. It has been shown that there is a high correlation between CBCT gray values and the real bone density;[24] however, the derived voxel gray values are dependent on the location of the object within the selected FOV and scanning parameters.[25,26] Owing to the mentioned instability of voxel gray values in CBCT, our samples were scanned with an identical position within the FOV and used the same scanning parameters.[20] Owing to severe artefacts in a few implants, selecting the ROI exactly adjacent to the implant body was difficult, so there were possibilities to have a distance (maximum, 0.5 mm) between the probe and implant. Therefore, in these cases part of the black shadows resulted from beam-hardening artefacts might be excluded. So, this could be a limitation of our study, as we might have missed part of the metal artefacts, which could affect the mean gray value measurements at the ROI. In the present study, an observer-independent and automated 3D-matching algorithm was used to make certain that gray value measurements were derived from identical ROI that are sub-voxel accurate. In comparison with previous *in vitro* studies, the use of a human dry mandible could better simulate the clinical setting. The physiological bone structures can cause scattering radiation that may not be accounted for in studies using a homogenous phantom.[27] However, artefacts from a cadaver or patient may vary from a dry bone, thus the MAR algorithm may perform differently. We excluded another source of artefact that might happen under normal clinical conditions: motion artefacts. Our results were limited to the applied FOV and scanning parameters, so further MAR assessments with different scanning factors are suggested.

In conclusion, the MAR tool in the ORTHOPANTOMOGRAPH OP300 CBCT scanner does not significantly correct the original voxel gray values in the vicinity of an implant. These empirical results agree with the theoretical results proving the limitation of 3D radiographic imaging techniques to visualize the close vicinity around dental implants, *e.g.* for post-operative assessment of osseointegration.

References

1. Ludlow JB, Laster WS, See M, Bailey LJ, Hershey HG. Accuracy of measurements of mandibular anatomy in cone beam computed tomography images. *Oral Surg Oral Med Oral Pathol Oral Radiol Endod* 2007; **103**: 534–42. doi: 10.1016/j.tripleo.2006.04.008
2. Song YD, Jun SH, Kwon JJ. Correlation between bone quality evaluated by cone-beam computerized tomography and implant primary stability. *Int J Oral Maxillofac Implants* 2009; **24**: 59–64.
3. Zhang Y, Zhang L, Zhu XR, Lee AK, Chambers M, Dong L. Reducing metal artifacts in cone-beam CT images by preprocessing projection data. *Int J Radiat Oncol Biol Phys* 2007; **67**: 924–32. doi: 10.1016/j.ijrobp.2006.09.045
4. Draenert FG, Coppenrath E, Herzog P, Müller S, Mueller-Lisse UG. Beam hardening artefacts occur in dental implant scans with the NewTom cone beam CT but not with the dental 4-row multidetector CT. *Dentomaxillofac Radiol* 2007; **36**: 198–203. doi: 10.1259/dmfr/32579161
5. Schulze R, Heil U, Gross D, Bruellmann DD, Dranischnikow E, Schwanecke U, et al. Artefacts in CBCT: a review. *Dentomaxillofac Radiol* 2011; **40**: 265–73. doi: 10.1259/dmfr/30642039
6. Kalender WA, Hebel R, Ebersberger J. Reduction of CT artifacts caused by metallic implants. *Radiology* 1987; **164**: 576–7. doi: 10.1148/radiology.164.2.3602406
7. Bal M, Spies L. Metal artifact reduction in CT using tissue-class modeling and adaptive prefiltering. *Med Phys* 2006; **33**: 2852–9.
8. Veldkamp WJ, Joemai RM, van der Molen AJ, Geleijns J. Development and validation of segmentation and interpolation techniques in sinograms for metal artifact suppression in CT. *Med Phys* 2010; **37**: 620–8.
9. Wang G, Snyder DL, O'Sullivan JA, Vannier MW. Iterative deblurring for CT metal artifact reduction. *IEEE Trans Med Imaging* 1996; **15**: 657–64. doi: 10.1109/42.538943
10. De Man B, Nuyts J, Dupont P, Marchal G, Suetens P. An iterative maximum-likelihood polychromatic algorithm for CT. *IEEE Trans Med Imaging* 2001; **20**: 999–1008. doi: 10.1109/42.959297
11. Schulze RK, Berndt D, d'Hoedt B. On cone-beam computed tomography artifacts induced by titanium implants. *Clin Oral Implants Res* 2010; **21**: 100–7. doi: 10.1111/j.1600-0501.2009.01817.x
12. Wang Q, Li L, Zhang L, Chen Z, Kang K. A novel metal artifact reducing method for cone-beam CT based on three approximately orthogonal projections. *Phys Med Biol* 2013; **58**: 1–17. doi: 10.1088/0031-9155/58/1/1
13. Bechara B, Alex McMahan C, Moore WS, Noujeim M, Teixeira FB, Geha H. Cone beam CT scans with and without artefact reduction in root fracture detection of endodontically treated teeth. *Dentomaxillofac Radiol* 2013; **42**: 20120245. doi: 10.1259/dmfr.20120245
14. Kamburoglu K, Kolsuz E, Murat S, Eren H, Yüksel S, Paksoy CS. Assessment of buccal marginal alveolar peri-implant and periodontal defects using a cone beam CT system with and without the application of metal artefact reduction mode. *Dentomaxillofac Radiol* 2013; **42**: 20130176. doi: 10.1259/dmfr.20130176
15. Bechara BB, Moore WS, McMahan CA, Noujeim M. Metal artefact reduction with cone beam CT: an *in vitro* study. *Dentomaxillofac Radiol* 2012; **41**: 248–53. doi: 10.1259/dmfr/80899839
16. Benic GI, Mokti M, Chen C-J, Weber H-P, Hammerle CHF, Gallucci GO. Dimensions of buccal bone and mucosa at immediately placed implants after 7 years: a clinical and cone beam computed tomography study. *Clin. Oral Impl. Res* 2012; **23**: 560–66.
17. Schropp L, Wenzel A, Spin-Neto R, Stavropoulos A. Fate of the buccal bone at implants placed early, delayed, or late after tooth extraction analyzed by cone beam CT: 10-year results from a randomized, controlled, clinical study. *Clin. Oral Impl. Res* 2014; 1–9.
18. Bechara B, McMahan CA, Geha H, Noujeim M. Evaluation of a cone beam CT artefact reduction algorithm. *Dentomaxillofac Radiol* 2012; **41**: 422–8. doi: 10.1259/dmfr/43691321
19. Ballhausen H, Reiner M, Ganswindt U, Belka C, Söhn M. Post-processing sets of tilted CT volumes as a method for metal artifact reduction. *Radiat Oncol* 2014; **9**: 114. doi: 10.1186/1748-717X-9-114.
20. Jaju PP, Jain M, Singh A, Gupta A. Artefacts in cone beam CT. *Open J Stomatol* 2013; **3**: 292–7. doi: 10.4236/ojst.2013.35049
21. Sarment D. *Cone beam computed tomography: oral and maxillofacial diagnosis and applications*. 1st edn. Hoboken, NJ: Wiley-Blackwell; 2013.
22. Pauwels R, Stamatakis H, Bosmans H, Bogaerts R, Jacobs R, Horner K, et al. Quantification of metal artifacts on cone beam computed tomography images. *Clin Oral Implants Res* 2013; **24** (Suppl. A100): 94–9. doi: 10.1111/j.1600-0501.2011.02382.x
23. Haramati N, Staron RB, Mazel-Sperling K, Freeman K, Nickoloff EL, Barax C, et al. CT scans through metal scanning technique versus hardware composition. *Comput Med Imaging Graph* 1994; **18**: 429–34.
24. Parsa A, Ibrahim N, Hassan B, Motroni A, van der Stelt P, Wismeijer D. Reliability of voxel gray values in cone beam computed tomography for preoperative implant planning assessment. *Int J Oral Maxillofac Implants* 2012; **27**: 1438–42.
25. Parsa A, Ibrahim N, Hassan B, van der Stelt P, Wismeijer D. Influence of object location in cone beam computed tomography (NewTom 5G and 3D Accuitomo 170) on gray value measurements at an implant site. *Oral Radiol* 2014; **30**: 153–9.
26. Parsa A, Ibrahim N, Hassan B, Motroni A, van der Stelt P, Wismeijer D. Influence of cone beam CT scanning parameters on grey value measurements at an implant site. *Dentomaxillofac Radiol* 2013; **42**: 79884780. doi: 10.1259/dmfr/79884780
27. Mah P, Reeves TE, McDavid WD. Deriving Hounsfield units using grey levels in cone beam computed tomography. *Dentomaxillofac Radiol* 2010; **39**: 323–35. doi: 10.1259/dmfr/19603304